Jurnal Kejuruteraan (*Journal of Engineering*) Submission DOI XXX 8 pages
ISSN:0128-0198 E-ISSN:2289-7526

Zero-Dimensional Single-Zone Combustion Modeling of an SI Engine Fuelled with Alcohol-Gasoline Blends

M. Firdaus Ayub[a], Syahar Shawal[a,*], Mohd Hanif Mat Muhammad[a], Juri Saedon[a], Nor Hafiez Mohamad Nor[a], Mohd Rosdzimin Abdul Rahman[b]

[a]*School of Mechanical Engineering, College of Engineering, Universiti Teknologi MARA, 40450 Shah Alam, Selangor, Malaysia*
[b]*Department of Mechanical Engineering, Faculty of Engineering, Universiti Pertahanan Nasional Malaysia, Kem Sg. Besi, 57000, Kuala Lumpur, Malaysia*

ABSTRACT

This study analysed and compared the combustion characteristics of baseline gasoline (M0) and methanol-gasoline blended with a 10% concentration (M10) in an SI engine using a zero-dimensional, single-zone combustion model. The experiments were performed in a production 4-cylinder, 4-stroke spark-ignition engine with premixed stoichiometric combustion. In the current work, the engine operated at 2000 rpm and 75Nm of torque. The crank-angle resolved pressure in the intake, exhaust, and in-cylinder was recorded in all experiments. An in-house algorithm was developed in MATLAB to derive the rate of heat release (RoHR) and evaluate mass fraction burned (MFB) curves from the measured in-cylinder pressure data of the two fuels. The effect of various heat transfer correlations—Annand, Hohenberg, and Woschni— on the heat release rate was also studied to identify the most suitable model for the specific SI engine. The results indicated that the methanol-blended fuel (M10) provided a higher RoHR compared to conventional gasoline fuel (M0). The MFB profile curves revealed the combustion progress of the fuels as a function of crank angle. The Hohenberg heat transfer model was better suited for heat transfer to the wall of the engine compared to the other models, as it gave the best fit in the compression phase. The addition of methanol to gasoline results in an increase in the combustion rate at CA10 (10% MFB) due to its higher flame speed propagation and octane rating.

Keywords: Zero-dimensional model; Combustion; Heat release rate; SI engine; Alternative fuel

INTRODUCTION

The inception of internal combustion engines (ICEs) marked a significant revolution in engineering. Most internal combustion vehicles still rely on conventional fuels derived from fossil sources such as gasoline or diesel (Köten, Karagöz, and Balcı 2020). These conventional fuels emit harmful substances, including carbon dioxide (CO_2) and nitrous oxide (N_2O), which contribute to air pollution and global warming. The increasing demand for petroleum has led to concerns not only about the depletion of reserves but also about the environmental pollution caused by conventional fuels (Sarkar et al. 2012). Consequently, optimizing internal combustion engines (ICEs) has become a critical area of research, with recent efforts focusing on enhancing engine efficiency and stability while reducing emissions (Dabbaghi et al. 2021).

The primary criticisms of internal combustion engines (ICEs) relate to their environmental impact and the challenges they present (Dabbaghi et al. 2021). Various approaches have been explored to address these issues, including the pursuit of alternative fuels derived from renewable resources. The United Nations has mandated that countries reduce their CO_2 emissions, prompting researchers to explore biofuels such as ethanol and methanol (Sharudin et al. 2018). The practice of blending low concentrations of methanol and ethanol with conventional fuels is not new; it was used during the oil supply shortages of the 1970s (Iliev 2015). One of the appealing aspects of blending ethanol and methanol with conventional fuels is that it can be done without significant modifications to the engine structure (Iliev 2015; Chansauria and Mandloi 2018).

Methanol, the simplest alcohol with the chemical formula CH_3OH, can be produced from various renewable and waste resources, including agricultural by-products and fossil feedstocks like coal and natural gas, with the latter being the primary source (Li et al. 2017). In contrast, ethanol production primarily involves the fermentation and distillation of biomass, such as crops (Eyidogan et al. 2010). Both methanol and ethanol have significantly higher octane numbers and latent heat of vaporization than conventional fuels, allowing for higher compression ratios and increased thermal efficiency, which is desirable for spark-ignited (SI) engines (Eyidogan et al. 2010; Black 1991). This is

because methanol and ethanol contain hydrogen, carbon, and oxygen, whereas conventional fuels primarily consist of hydrogen and carbon (Black 1991). The compositional difference of baseline, ethanol and methanol fuels characteristics are shown in the Table 1.

TABLE 1. Characteristics of baseline, methanol and ethanol fuels (Black 1991; Eyidogan et al. 2010)

Characteristics	Baseline (RON 95)	Methanol	Ethanol
Typical formula	C_8H_{18}	CH_3OH	C_2H_6OH
Research Octane Number (RON)	91-100	112	111
Heat of vaporisation (kJ/kg)	400	1,110	900
Stoichiometric A/F [9]	14.5	6.4	9
Heating value (kJ/kg) [8]	42.6	26.7	19.85

Table 1 indicates that methanol and ethanol share similar Research Octane Numbers (RON) and possess high latent heat of vaporization, as well as lower stoichiometric air-fuel ratios and heating values compared to baseline fuel, although there are slight variations between the two. These characteristics are due to the fact that methanol and ethanol belong to the alcohol family, which includes compounds with higher oxygen content in their chemical structures, enhancing fuel performance (Iliev 2015; Chen et al. 2019). Consequently, these attributes are maintained when methanol and ethanol are blended with baseline fuel. Blending high-octane, oxygenated ethanol and methanol with conventional fuel is crucial as it results in an increase in the research octane number. As noted by M. Eyidogan et.al (2010), every 10% addition of alcohol fuel can raise the octane number by up to five units (Eyidogan et al. 2010). This increase is attributed to their ability to reduce engine knocking, which is a result of their higher RON. Moreover, alcohol-blended fuels have been found to decrease CO_2 emissions . Research suggests that using alcohol fuels with higher RON values enables SI engines to operate at higher compression ratios, leading to greater combustion pressure and torque output.

The addition of oxygen in the fuel has been observed to affect ignition and early flame propagation, which in turn modifies the in-cylinder pressure profile (Shawal, S., et al. 2016). The optical studies revealed that turbulent flame propagation was influenced by the ignition plasma and the formation of the early kernel during the initial phase of combustion (Shawal, S., et al. 2020). In-cylinder pressure can be analysed thermodynamically using the rate of heat release (RoHR), which is based on the first law of thermodynamics (Heywood 1988). RoHR analysis is important because it establishes a correlation between pressure variations and the chemical energy released during combustion. The pressure-derived mass fraction burned (MBF) shows a good correlation with the optically determined flame speed obtained from high-speed imaging technique (Shawal, S., et al. 2020). The RoHR is defined as the rate at which chemical energy is released during combustion (Rosdi et al. 2022). RoHR analysis models can be classified into single-zone and two-zone models. The single-zone model is simpler as it treats the cylinder contents as a homogeneous mixture, whereas the two-zone model distinguishes between burnt and unburnt gases (Heywood 1988). The integral of RoHR provides the mass fraction burned (MFB), an S-shaped curve that represents the percentage of fuel consumed relative to crank angle, which is used to characterize the spark ignition combustion process [(Cooney, Worm, and Naber 2008). Despite the simplicity of the single-zone model, the combustion analysis results are nearly identical to those of the two-zone model, as suggested by Cooney, Worm and Naber (2008) in their study on the calculation of mass fraction for ethanol-gasoline using both models (Cooney, Worm, and Naber 2008). They concluded that the MFB results from both models were approximately the same when accounting for heat transfer.

Several studies have investigated the combustion characteristics of various alcohol-blended fuels compared to baseline fuels in both spark ignition (SI) and diesel engines. Qi and Lee (2016) found that ethanol blends affect in-cylinder pressure and RoHR, with higher ethanol content (e.g., E20) resulting in higher peaks at higher loads, similar to the MFB due to increased laminar flame speed (Qi and Lee 2016a). Alexander and Porpatham (2019) concluded that a 10% ethanol blend with LPG showed better RoHR and in-cylinder pressure compared to baseline fuels and other blends (Alexander and Porpatham 2019). (Köten, Karagöz, and Balcı (2020) observed that increasing ethanol concentration in gasoline led to higher cylinder pressure, RoHR, power, and torque

due to ethanol's lower stoichiometric ratio, which allows more fuel mass to combust compared to standard gasoline (Köten, Karagöz, and Balcı 2020). Chen et al. (2019) noted that methanol/gasoline blends resulted in higher peak cylinder pressure, temperature, and RoHR with increased methanol content, attributing this to faster flame development and propagation (Chen et al. 2019). Li et al. found that alcohol-blended fuels advanced combustion phasing due to their high laminar flame speed and shorter ignition delay, owing to their high latent heat of vaporization (Li et al. 2017). Huang et al. observed that methanol-blended fuels in diesel engines increased in-cylinder pressure and RoHR, particularly at higher loads, with shorter ignition delays due to methanol's low autoignition temperature (Huang et al. 2020).

Numerous research studies have explored the impact of different concentrations of alcohol-blended fuel on baseline fuels, including the effect of various heat transfer correlations on SI engine performance. According to Heywood (1988), heat transfer is particularly crucial when temperatures peak towards the end of combustion, as it plays an essential role in the overall energy transfer and thermal management of the system, even though it constitutes only a small fraction of the fuel's energy (Heywood 1988). Heat transfer to the cylinder wall is a vital aspect of the overall energy management system (Heywood 1988). The study by Dabbaghi et al. (2021) investigates the impact of various heat transfer correlations—namely Annand, Hohenberg, Woschni, and Sitkei's correlations—on an SI crank-rocker engine (Dabbaghi et al. 2021). A study by Aziz Hairuddin, Wandel, and Yusaf (2013) examined the effects of different heat transfer methods on HCCI engine performance, using the Hohenberg, Woschni, and Modified Woschni models (Aziz Hairuddin, Wandel, and Yusaf 2013). In the study conducted by Meena, Pal and Gautam (2022), the net heat release rate was used instead of the total RoHR for evaluating combustion characteristics (Meena, Pal, and Gautam 2022). For simplicity, the influence of heat transfer was not considered in the net RoHR usage.

Therefore, the aims of this project are to analyze and compare the combustion characteristics of baseline gasoline (M0) and a methanol-gasoline blend with a 10% concentration (M10) in a production spark-ignited engine using a zero-dimensional, single-zone combustion model. Three different models of heat loss to the cylinder wall (Woschni, Annand, and Hohenberg) were tested and compared based on the total rate of heat release and the fitness in the compression phase. This project aims to visualize the pressure and combustion profiles of different fuels and derive the rate of heat release over the crank angle (combustion period) for hundreds of combustion cycles.

METHODOLOGY

Geometrical properties of the engine

The experiments were carried out in a production 4-cylinder 4-stroke spark-ignition engine with premixed stoichiometric combustion. In the current work, the engine operated at 2000 rpm and 75Nm of torque. To achieve this load, 4.4 bar IMEP, at 1000 mbar intake pressure, the ECU set a maximum intake valve lift of 2.2 mm. The ignition timing was automatically adjusted by the Engine Control Unit (ECU) at 34.5° CA bTDC. The crank-angle resolved pressure in the intake, exhaust, and in-cylinder were recorded in all experiments. Table 2 shows the engine parameters used to determine the geometrical properties in the analysis.

TABLE 2. Engine parameters

Compression ratio, -	10
Connecting rod length to crank radius, mm	22.2
Stroke, mm	90
Crank radius, mm	45
Bore, mm	84
Speed, RPM	2000
Torque, Nm	75
Fuel	M0/M10
Intake valve close, IVC	-175.7°
Exhaust valve open, EVO	179.5°
Exhaust valve close, EVC	-404.5°
Intake pressure, mbar	1000

Cylindrical volume, V

The cylinder volume at any crank angle, θ is given as:

$$V = V_c + \frac{\pi D}{4}(R + a - s) \quad (1)$$

Where V_c is the clearance volume, V_d is the displacement volume, and s is the distance between the crank axis and the piston pin, defined as

$$s = acos\theta + (R^2 - a^2 sin^2\theta)^{1/2} \quad (2)$$

Substituting s into (1) yields

$$V = V_c * [1 + (\frac{r_c - 1}{2}) * (R + 1 - cos\ \theta\ - (R^2 - sin^2\theta)^{1/2}] \quad (3)$$

Temperature model

The temperature model used in the project was based on the ideal gas state equation, which is described in crank angles basis. The equation is stated below

$$PV = mR_{gas}T \quad (4)$$

Where P is the in-cylinder pressure measured using a piezoelectric transducer, V is the volume of the engine at any crank angle, m is the residual mass, R_{gas} is the gas constant, and T is the average gas temperature. Rearrange the equation into

$$T = \frac{PV}{mR_{gas}} \quad (5)$$

The instantaneous cylinder volume was pre-determined during the in-cylinder pressure data collection, where the volume was determined with a resolution of 0.5° crank angle.

Polytropic index,n

The polytropic index was used to describe the adiabatic process of A/F mixture during the compression cycle, where the temperature of the mixture increased without any heat lost the cylinder wall. The polytropic index, n of the A/F mixture, was described using the relationship of pressure and volume during the compression cycle.

$$PV^n = constant \quad (6)$$

$$n = constant\left(\frac{P_1V_1}{P_2V_2}\right) \quad (7)$$

Specific Heat Ratio, γ

The specific heat ratio, gamma was computed based on a linear model (Brunt, Rai, and Emtage 1998). The γ model is modelled as a linear function of temperature.

$$\gamma(T) = 1.345 - (4.78 \times 10^{-5}) * T \quad (8)$$

Heat transfer model

The heat transfer to the cylinder wall is based on Newton's law of cooling or convective heat transfer, as it provides a significant impact in in-cylinder heat transfer, which is given

$$Q_w = hA(T - T_w) \quad (9)$$

Where h is the heat transfer coefficient, T is the in-cylinder gas mixture temperature, T_w is the cylinder wall temperature, and A is the cylinder chamber surface area (Chansauria and Mandloi 2018). Forced convection is more convenient to use as a heat transfer model due to the consequences of external mechanical action in the chamber that caused the fluid flows, as the radiation only suits a few engine types (Heywood 1988).

Three models of convective heat transfer coefficient, h were applied in the analysis: Annand, Hohenberg, and Woschni (Hohenberg 1979; Annand 1963; Woschni 1967).

Woschni's correlation

Woschni correlation is based on the convection heat transfer, which is the basic effect derived from the laws of similarity for turbulent flow in terms of Reynolds number and correlates it with Nusselt number. The correlation is as follows (Woschni 1967):

$$h_c = 3.26B^{-0.2} \times P^{0.8} \times w^{0.8} \times T^{-0.55} \quad (10)$$

Where B is the bore diameter of engine, p is the instantaneous pressure, w is the average cylinder gas velocity, and T is the instantaneous temperature. Woschni stated that $w(\theta)$ increases in the cylinder during combustion, compared to others, where it is constant. It is represented as below:

$$w(\theta) = C_1\bar{S}_p + C_2\frac{V_dT_r}{p_rV_r}(p\,(\theta)\ -\ p_m)^n \quad (11)$$

$$p_m = p_r\left(\frac{V_r}{V(\theta)}\right) \quad (12)$$

Where C_1 and C_2 are constants and taken as 2.28 and 3.24 x 10^{-3}, for the combustion and compression respectively. $\bar{S}_p$ is the mean piston speed, V_d is the displacement volume, p_r is the reference gas pressure, V_r is the reference gas volume, p is the instantenous in-cylinder pressure, p_m is the motored pressure, and V is the instantenous volume.

Hohenberg's correlation

Woschni correlation exhibits certain limitations as it tends to underestimate the compression process while overestimating the combustion process in relation to the heat transfer coefficient. This leads to an excessive average heat flux throughout the cycle (Hairuddin, Yusaf, and Wandel 2016). Hohenberg made a substitute for providing a more accurate prediction of time-averaged heat fluxes, measured with the usage of length based on instantaneous cylinder volume and mean piston speed rather than the cylinder bore, as well as in the exponent of temperature term. The changes in the heat transfer coefficient as shown below:

$$h_c = C_1 \times V_c^{-0.06} \times P^{0.8} \times T^{-0.4}\left(C_2 + \bar{S}_p\right)^{0.8} \quad (13)$$

C_1 and C_2 values are denoted with h values of 130 and 1.4, obtained using precise and detailed measurements of different engines' heat balance, heat flux, and component temperature. V_c is cylinder volume, p is the instantaneous pressure, T is the instantaneous temperature, and $\bar{S}_p$ is the mean piston speed.

Annand's correlation

Annand produced a model to anticipate the heat transfer using Newtonian and the Nusselt and Reynold numbers, where he separates the heat transfer coefficient into the convective and radiative heat transfer coefficients. The correlation is stated below:

$$h_g = a \times \frac{k_{gas} Re^{0.7}}{B} + c.\sigma \frac{(T^4 - T_w^4)}{(T - T_w)} \quad (14)$$

where

$$k_{gas} = 6.1944x10^{-3} + 7.3814\,x\,10^{-5}T - 1.2491x10^{-8} \quad (15)$$

B is bore of the cylinder, ρ is the density of the fuel that is calculated using ideal gas law, μ is dynamic viscosity with an approximate value of 7 x 10^5 kg/ms, and $\bar{S}_p$ is the mean piston speed. k_{gas} refers to the gas thermal conductivity modelled using a polynomial curve-fitting of the measured data. The constant a varies within the range of 0.35 – 0.8 for standard operating conditions, where it relies on the intensity of charge motion. The value of c is equivalent to 0.075 for SI engines during combustion and expansion phase. Stefan-Boltzmann constant, σ is given as 5.67 x 10^{-8} W/m^2. K^4. T is the instantaneous in-cylinder temperature and T_w is the wall temperature of the cylinder.

All three models are tabulated in the Table 3 below:

TABLE 3. Heat transfer correlations

Woschni	$3.26B^{-0.2} \times P^{0.8} \times w^{0.8} \times T^{-0.55}$
Hohenberg	$C_1 \times V_c^{-0.06} \times P^{0.8} \times T^{-0.4}\left(C_2 + \bar{S}_p\right)^{0.8}$
Annand	$a \times \frac{k_{gas} Re^b}{B} + c.\sigma \frac{(T^4 - T_w^4)}{T - T_w)}$

Rate of Heat Release (RoHR)

Zero-dimensional engine modelling's most straightforward approach is the in-cylinder content regarded as a single zone and uses the first principle of thermodynamics with an ideal gas state equation, in which the heat transfer effect to the wall can be integrated into the equation (Yıldız and Albayrak Çeper 2017). The first law of thermodynamics states

$$\Delta U_{sys} = Q_{net} - W_{net} \quad (16)$$

$$Q_{net} = Q_b - Q_w \quad (17)$$

Where ΔU_{sys} is the change in internal energy, Q_{net} is the net heat transfer to the system, and W_{net} is the net work done by the system.

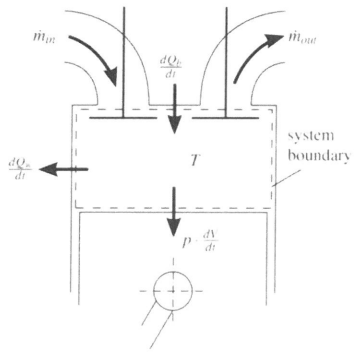

FIGURE 1. First law of thermodynamics assumptions (Heywood 1988)

$$Q_b = \Delta U + Q_w + W_{net} \quad (18)$$

The derivation of RoHR was based on the first law of thermodynamic in the combustion chamber as shown in the Figure 1. ΔU and W_{net}, which are defined as:

$$\Delta U = mc_v dT \quad (19)$$

$$W_{net} = PdV \quad (20)$$

Substituting the thermodynamic expression into the first law of the open system:

$$Q_b = mC_v dT + Q_{ht} + PdV \quad (21)$$

$$dT = \frac{VdP}{mR} \quad (22)$$

$$dT = \frac{PdV}{mR} \quad (23)$$

Substituting Eq. 22 and Eq. 23 into Eq.21 yield:

$$Q_b = \frac{C_v}{R} VdP + \left(\frac{C_v}{R} + 1\right) PdV + Q_w \quad (24)$$

Where Q_w is the heat transfer to the cylinder wall. Specific gas constant equation, Eq.25 and specific heat ratio, γ, equation, Eq.26 were substituted into Eq.24. Thus, the derivation of the RoHR is shown as Eq.27.

$$C_p - C_v = R \quad (25)$$

$$\frac{C_p}{C_v} = \gamma \quad (26)$$

$$Q_b = \frac{1}{\gamma - 1} VdP + \frac{\gamma}{\gamma - 1} pdV + Q_w \quad (27)$$

Eq.27 was differentiated with respect to time (crank angle), as shown in Eq.28.

$$\frac{dQ_b}{d\theta} = \frac{1}{\gamma - 1} V \frac{dP}{d\theta} + \frac{\gamma}{\gamma - 1} P \frac{dV}{d\theta} + \frac{dQ_w}{d\theta} \quad (28)$$

Mass fraction burned (MFB)

Mass fraction burned (MFB) is the energy-release fraction as a function of crank angle in each individual cycle, which has the characteristic of an S-shaped shape (Cooney, Worm, and Naber 2008; Heywood 1988). The combustion of fuel-air mixture exhibits a characteristic trend wherein the combustion rate initially increases after spark discharge, reaches a peak during the midway of the combustion process, and subsequently decreases to near-zero levels upon completion of combustion. The utilization of mass fraction burned or energy-release fraction curves is a viable approach to visually represent the temporal characteristics of different phases of the combustion process in spark-ignition engines. This method enables the precise determination of the engine cycle duration occupied by each phase.

The process of acquiring MFB is by summing the cumulative heat release through the integral of RoHR curve. The integral of the RoHR is normalised by dividing with the value of (m_f x Q_{LHV}).

$$CHR = \int_{\theta = IV0}^{\theta = IVC} (RoHR)\, d\theta \quad (29)$$

$$MFB = \frac{CHR}{m_f Q_{LHV}} \quad (30)$$

Algorithm procedures

The flow chart of the numerical algorithm is shown in Figure 2 below:

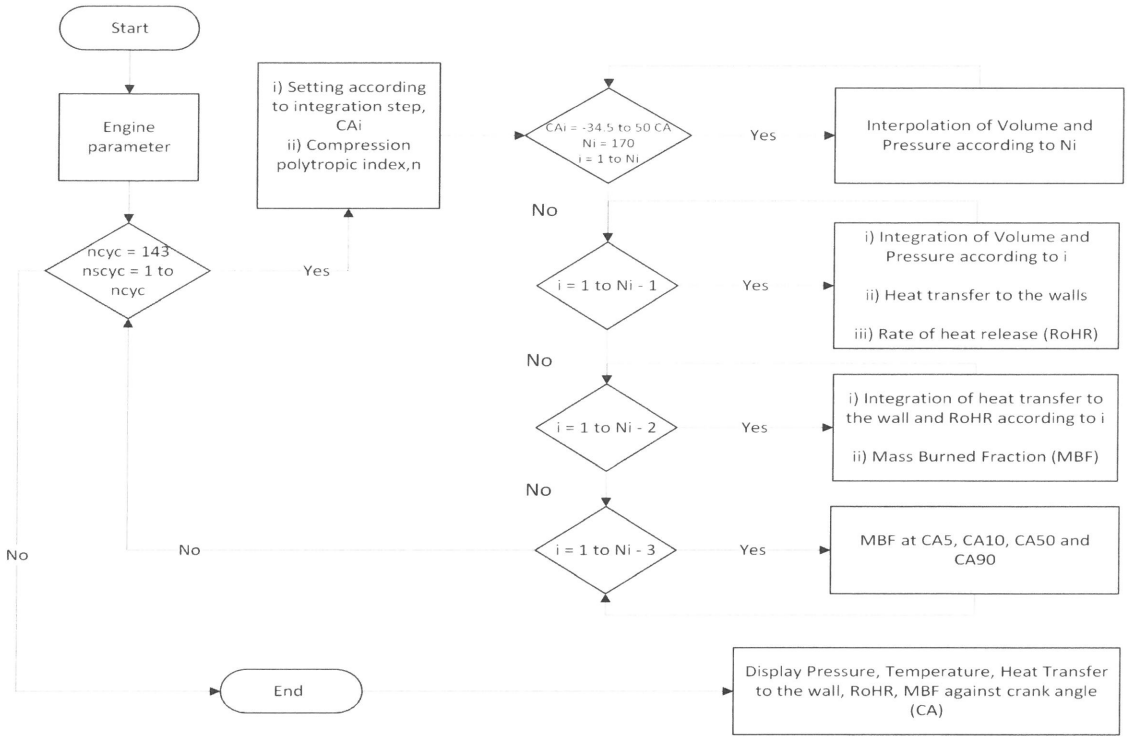

FIGURE 2. Algorithm flow chart of thermodynamic analysis

The process flow started with defining the engine parameters, such as the pressure and volume from the engine data. The simulation computed over 143 consecutive combustion cycles. The heat release integration period was calculated during -34.5 to 50 degrees at top dead centre (aTDC) with an increment of 0.5 degree.

RESULTS AND DISCUSSION

In-cylinder pressure

Figures 3 and 4 illustrate the in-cylinder pressure plotted against crank angle for both the baseline and methanol-blended fuels, with black lines representing the pressure data for each fuel over 143 cycles. Figure 5 provides a comparative analysis of the averaged pressure at after top dead center (aTDC) for the two fuels. The results indicate that methanol-blended fuel achieved a higher mean peak pressure at a lower crank angle compared to the baseline fuel. According to the results, variations in in-cylinder pressure were not distinctly observable at the start of ignition (SOI), approximately -30° to -10° aTDC, but became more dispersed during the combustion process.

The baseline fuel generated a peak average pressure of 3200 kPa at 7.5° aTDC, whereas the methanol-blended fuel produced a peak average pressure of 3300 kPa at 5.5° aTDC. The in-cylinder pressure for the methanol-blended fuel peaked 100 kPa higher and occurred 2° earlier aTDC than the baseline fuel. This phenomenon can be attributed to the characteristics of alcohol, which has a higher octane number, greater latent heat of vaporization, and higher laminar flame speed compared to pure gasoline (Paluri and Patel 2022). The high laminar flame speed of methanol promotes faster flame propagation, and its high latent heat of vaporization cools the air-fuel mixture, leading to more efficient combustion. Additionally, the air-fuel ratio affects in-cylinder pressure; methanol, with its lower stoichiometric air-fuel ratio due to the presence of oxygen in its chemical structure, requires less air for complete combustion (S.M Rosdi et al. 2022; Black 1991).

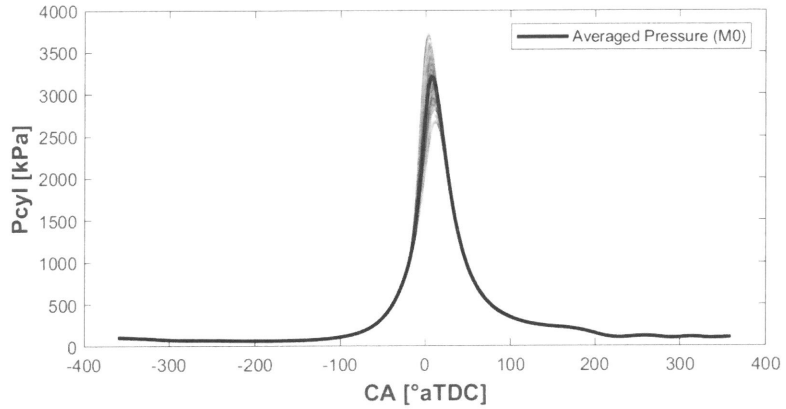

FIGURE 3. In-cylinder pressure traces of M0 fuel over 143 cycles

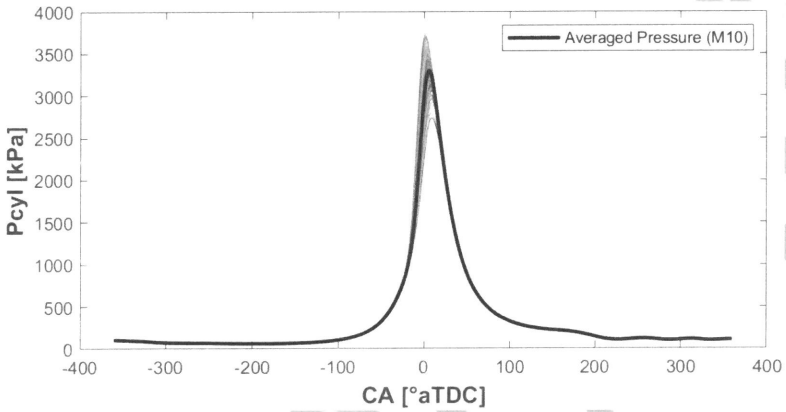

FIGURE 4. In-cylinder pressure traces of M10 fuel over 143 cycles

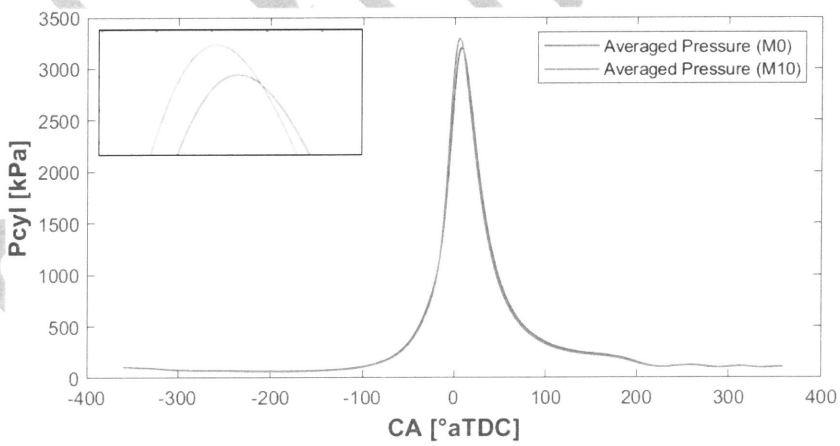

FIGURE 5. Averaged of in-cylinder pressure trace for both fuel over all cycles

To evaluate the relative variability or dispersion of the data, the peak pressure data over all cycles were statistically analyzed using the coefficient of variation (CoV) approach. CoV is calculated as the ratio of the standard deviation to the mean of the peak pressure data set, as shown as below:

$$CoV = \frac{\sigma\ of\ peak\ pressure}{mean\ of\ peak\ pressure} x100\% \quad (35)$$

The results derived from the analysis indicated that the peak pressure data for the baseline fuel, RON 95, exhibited higher variability or fluctuation compared to the methanol-blended fuel, with CoV values of 7.58% and 5.49%, respectively. These findings suggest that the methanol-blended

fuel demonstrated more consistent and precise peak pressure during the combustion process than the baseline fuel, corroborating the results obtained by Alexander and Porpatham (2019) (Alexander and Porpatham 2019). This consistency can be attributed to the higher oxygen content in alcohol fuels. Methanol, with its higher laminar flame speed and octane number, provides more efficient combustion (Alexander and Porpatham 2019; Chansauria and Mandloi 2018). The development and propagation of the flame pattern significantly impact combustion variations. Thus, higher combustion efficiency reduces the variability of peak in-cylinder pressure.

Heat transfer to the wall

Figures 6 and 7 illustrate the heat transfer to the cylinder wall for both baseline and methanol-blended fuels using the heat transfer correlations developed by Woschni, Hohenberg, and Annand. According to Figure 8, Hohenberg's correlation recorded the highest heat transfer to the wall for both the baseline and methanol-blended fuels, followed by Woschni's and Annand's correlations. The methanol-blended fuel also reached peak heat transfer significantly earlier than the baseline fuel. As shown in Table 4, the heat transfer for methanol-blended fuel peaked at 4.0°, 4.5°, and 4.5° after top dead center (aTDC) according to Hohenberg's, Woschni's, and Annand's correlations, respectively. In contrast, the heat transfer for the baseline fuel peaked at 5.5° aTDC across all correlations. The difference in peak heat transfer between the two fuels was approximately 1 to 1.5° aTDC, meaning that methanol-blended fuel achieved peak heat transfer 28% faster than the baseline fuel.

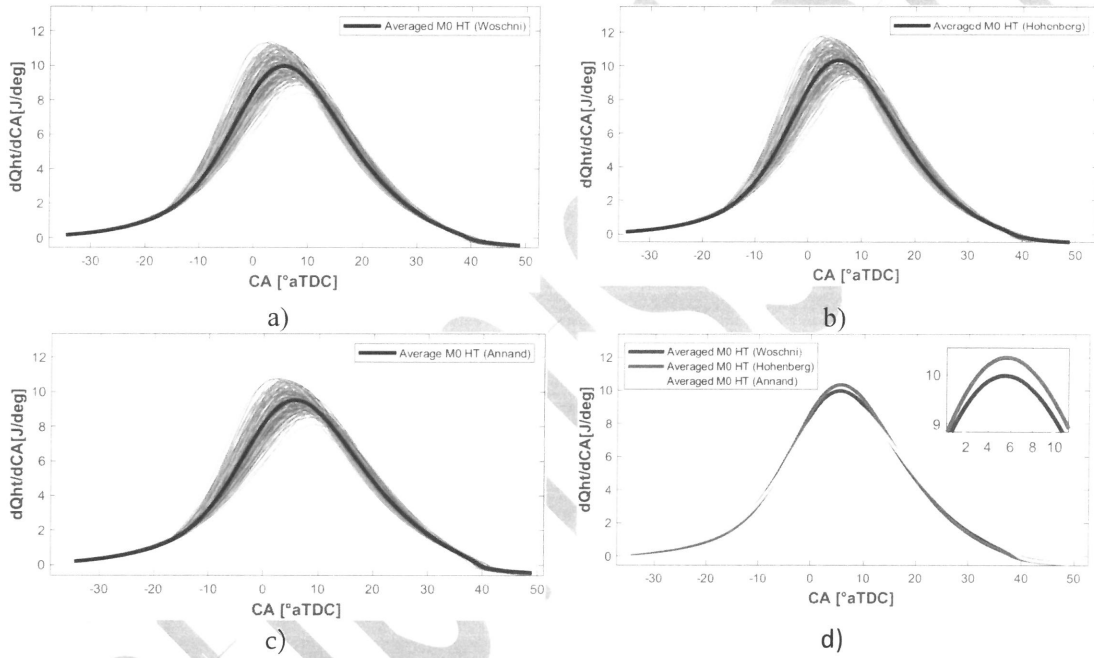

FIGURE 6. RON95 (M0) heat transfer to the wall using a) Woschni, b) Hohenberg, c) Annand and d) average of the three correlations

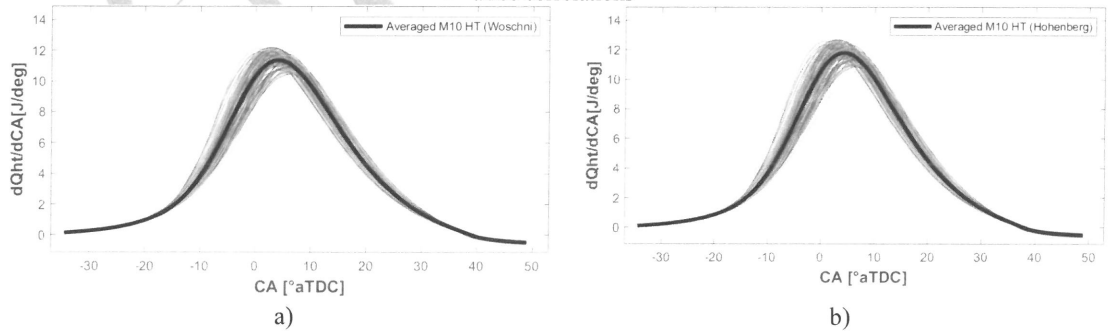

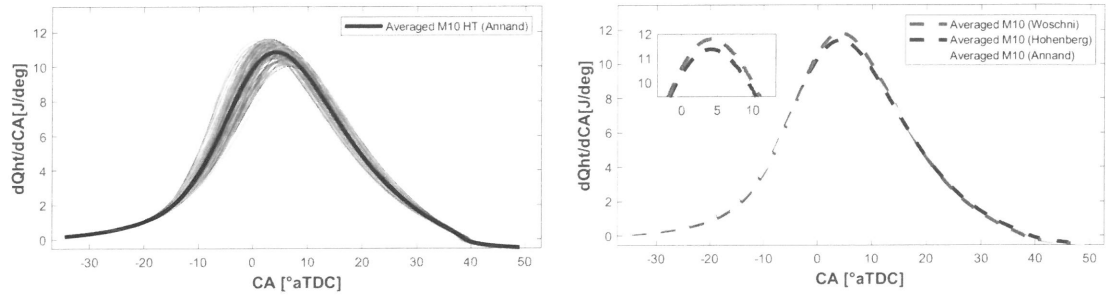

FIGURE 7. Methanol-blended fuel (M10) heat transfer to the wall using a) Woschni, b) Hohenberg, c) Annand and d) average of the three correlations over 143 cycles

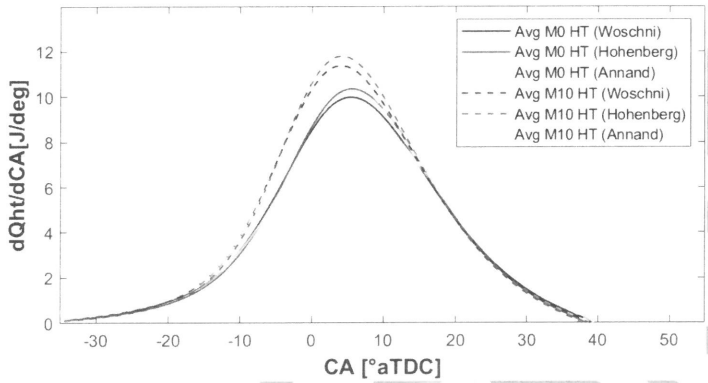

FIGURE 8. Averaged in-cylinder pressure for both fuel over one complete cycle

TABLE 4. Heat transfer correlations

	Baseline		Methanol-blended	
	dQ_{HT} (J/deg)	°aTDC (deg)	dQ_{HT} (J/deg)	°aTDC (deg)
Hohenberg	10.35	5.5	11.79	4.0
Woschni	9.98	5.5	11.37	4.5
Annand	9.52	5.5	10.83	4.5

Soyhan *et al.* (2009) found that several parameters impact the magnitude of heat transfer coefficients, including length scale, pressure, velocity, and gas temperature. They concluded that temperature influences only the magnitude of correlations, whereas the length scale affects both the magnitude and the shape of correlations. This effect of the length scale is evident in Hohenberg's modifications to Woschni's correlation, which originally had accuracy flaws leading to an underestimation of heat transfer coefficients during the compression process and an overestimation during the combustion process. Hohenberg replaced the bore with a length based on instantaneous cylinder volume, adjusted for changes in effective gas velocity, and modified the exponent of the temperature term.

Additionally, the heat transfer rate results demonstrated a difference between the two fuels, with methanol-blended fuel showing higher rates. This can be attributed to the fact that each correlation is influenced by pressure, temperature, or both, and methanol-blended fuel improved both variables due to its unique characteristics as a fuel. Previous studies have shown that alcohol-blended fuels, such as methanol, contain a higher proportion of oxygen compared to pure gasoline, RON 95 (Eyidogan et al. 2010; Sharma et al. 2019; Chen et al. 2019; Huang et al. 2020; Li et al. 2017). This increased oxygen content leads to higher pressure and temperature, which in turn affects the heat transfer correlations.

Rate of Heat Release (RoHR)

Figures 9 and 10 illustrate the rate of heat release (RoHR) for both baseline and methanol-blended fuels over 143 cycles. The figures indicate that Hohenberg's correlation provided the highest RoHR for both fuels among the correlations used. For the methanol-blended fuel, the highest heat release recorded was 33.40 J/degree at -2.5° after top dead center (aTDC) using Hohenberg's correlation, followed by 33.18 J/degree at -2.5° aTDC using Woschni's correlation, and 30.84 J/degree at -3.0° aTDC using Annand's correlation. For the baseline

fuel, the highest RoHR recorded was 38.11 J/degree at -3.0° aTDC using Hohenberg's correlation, followed by 31.74 J/degree at -0.5° aTDC using Woschni's correlation, and 30.80 J/degree at -0.5° aTDC using Annand's correlation. The RoHR more closely represents the chemical energy release when considering heat transfer, with the difference being due to combustion inefficiencies. A similar observation was made by A. Hairuddin *et al.*, who found that a high rate of heat transfer to the wall leads to an increased heat release rate. They noted that both Hohenberg's and Woschni's correlations assume that the characteristic velocity remains consistent throughout the strokes, which results in a significant amount of heat being transferred to the wall, thereby increasing the RoHR.

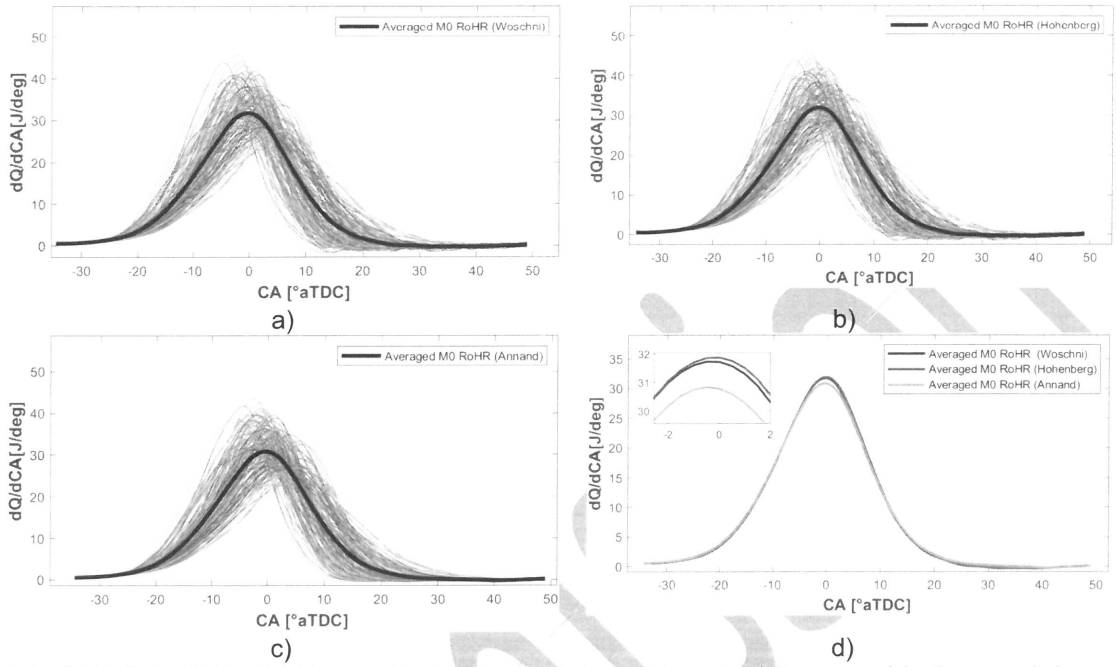

FIGURE 9. RON95 (M0) RoHR using a) Woschni, b) Hohenberg, c) Annand and d) average of the three correlations

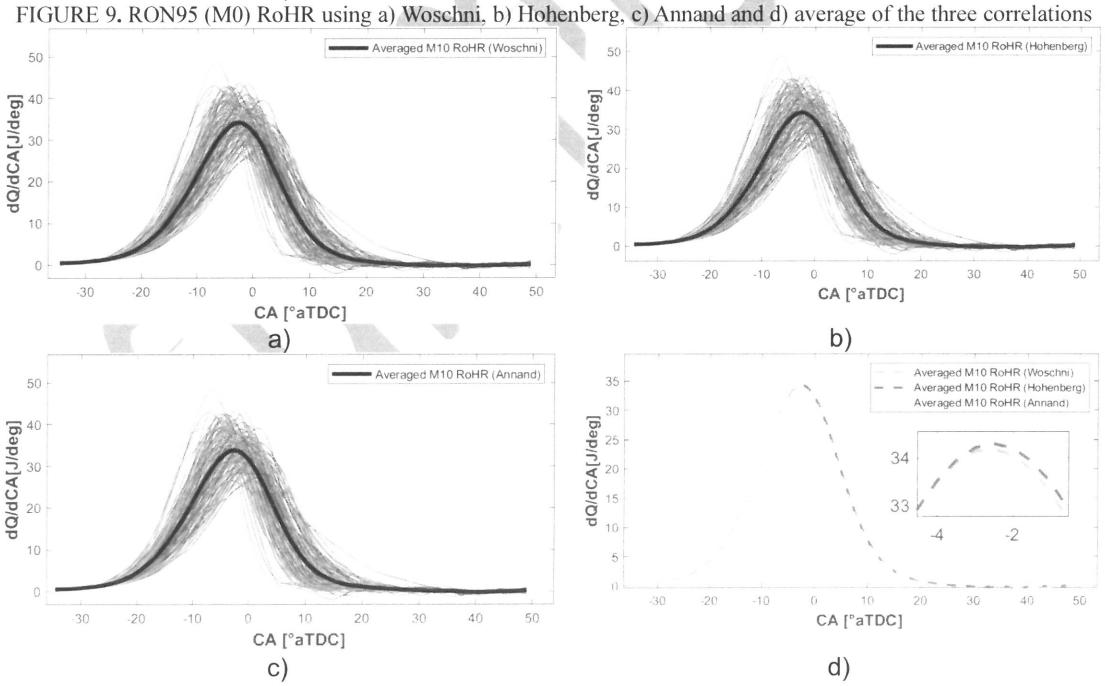

FIGURE 10. Methanol-blended fuel (M10) RoHR using a) Woschni, b) Hohenberg, c) Annand and d) average of the three correlations over 143 cycles

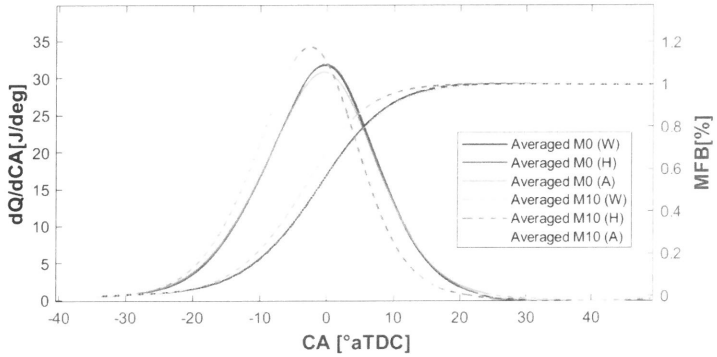

FIGURE 11. Comparison of average RoHR and MFB between two fuels across all correlations

Figure 11 shows that the rate of heat release (RoHR) peak occurred slightly earlier for the methanol-blended fuel, as its curves shifted to the left, indicating the peak before the piston reached top dead center (TDC). In contrast, the RoHR peak for the baseline fuel occurred after TDC. According to the data tabulated in Table 5, methanol-blended fuel exhibits a higher RoHR than the baseline fuel. The RoHR for methanol-blended fuel shifted 2.0° aTDC earlier than that of the baseline fuel for all correlations. When comparing the baseline fuel with the methanol-blended fuel, it was observed that the latter reached its RoHR peak approximately 80% sooner. These findings suggest that the properties of the fuel and the mechanisms of heat transfer significantly influenced the results. Alcohol fuels have a higher laminar flame speed, which accelerates the combustion process during the early phase of combustion. Additionally, the presence of hydroxyl groups in the methanol molecule weakens the molecular bonds of the baseline fuel, leading to a lower temperature at which oxidation occurs. This accelerated oxidation process enhances combustion.

TABLE 5. Rate of heat release (RoHR) for both fuels with different correlations

	Baseline		Methanol-blended	
	dQ_{ch} (J/deg)	°aTDC (deg)	dQ_{ch} (J/deg)	°aTDC (deg)
Hohenberg	31.88	-0.5	34.40	-2.5
Woschni	31.74	-0.5	33.84	-2.5
Annand	30.84	-0.5	33.11	-2.5

Mass Fraction Burned

Figures 12 and 13 illustrate the mass fraction burned (MFB) for both the baseline and methanol-blended fuels over 143 cycles. The average MFB for each fuel is highlighted in black to better depict the amount of fuel burned during combustion. Figure 14 compares the average MFB of both fuels across all correlations over the 143 cycles. The MFB curve effectively represents the flame burning progress of each fuel.

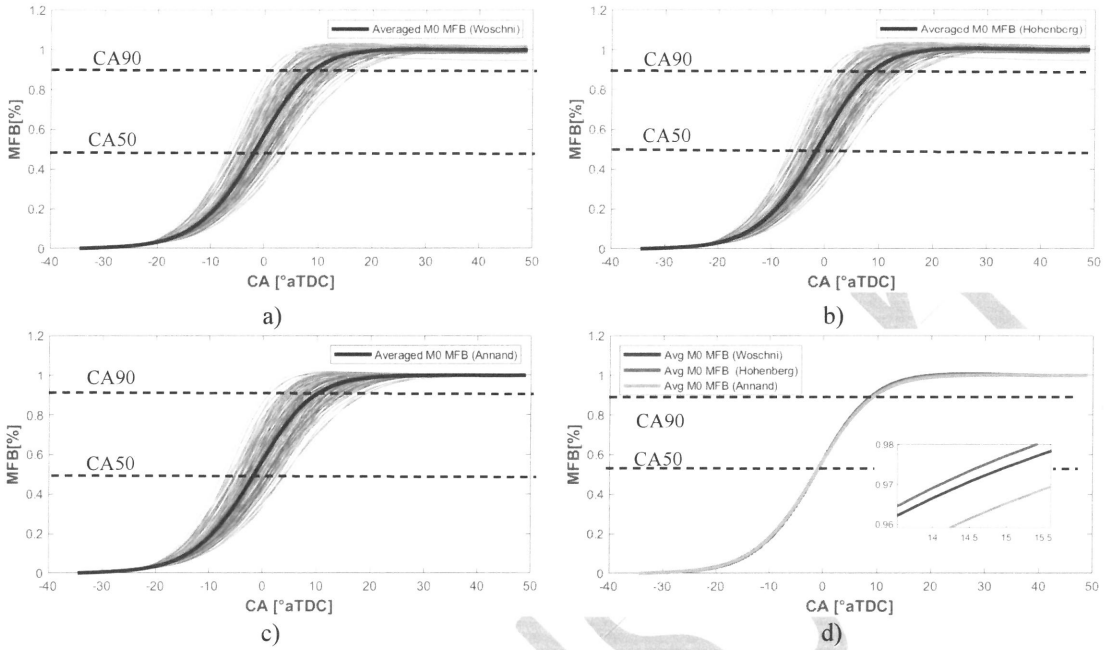

FIGURE 12. RON95 fuel (M0) MFB using a) Woschni, b) Hohenberg, c) Annand and d) average of the three correlations

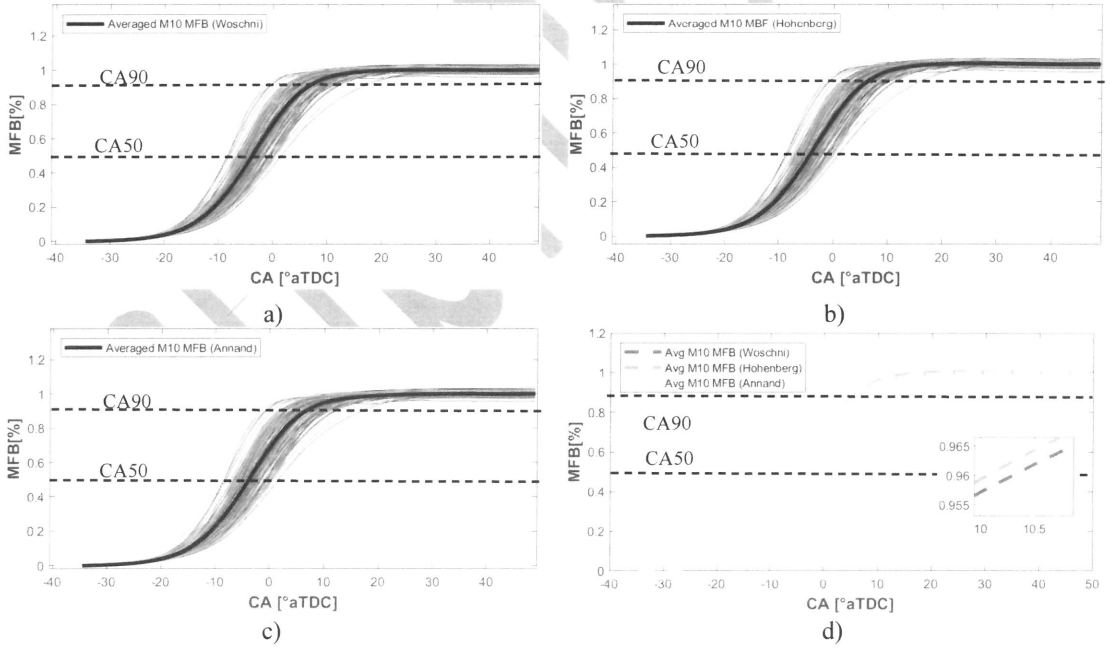

FIGURE 13. Methanol-blended fuel (M10) MFB using a) Woschni, b) Hohenberg, c) Annand and d) average of the three correlations over 143 cycles

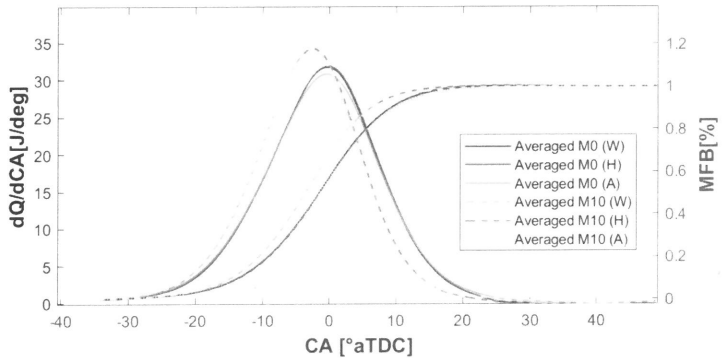

FIGURE 14. Comparison of average RoHR and MFB between two fuels across all correlations

TABLE 6. Heat transfer to the wall for both fuels using different correlations

	Baseline (M0)		**Methanol-blended (M10)**	
Woschni	MFB (%)	°aTDC (deg)	MFB (%)	°aTDC (deg)
	5	-16.5	5	-17.0
	10	-12.0	10	-13.0
	50	2.5	50	-2.0
	90	13.5	90	6.5
Hohenberg	MFB (%)	°aTDC (deg)	MFB (%)	°aTDC (deg)
	5	-16.0	5	-17.0
	10	-11.5	10	-13.0
	50	2.5	50	-2.0
	90	13.5	90	6.5
Annand	MFB (%)	°aTDC (deg)	MFB (%)	°aTDC (deg)
	5	-16.5	5	-17.5
	10	-12.0	10	-13.0
	50	2.5	50	-2.0
	90	14.0	90	7.0

Figure 14 illustrates the fuel burn progression for both baseline and methanol-blended fuels, with the latter shifting to the left, consistent with the previously discussed rate of heat release (RoHR) trend. Table 6 shows that the mass fraction burned (MFB) based on the Hohenberg correlation at CA50 occurred at 2.5° aTDC for the baseline fuel and -2.0° aTDC for the methanol-blended fuel. This indicates that the MFB for methanol-blended fuel advanced compared to the baseline fuel. In the early combustion phase, methanol-blended fuel showed faster progression, with a slight advancement of about 0.5 to 1.0° aTDC. This advancement became more apparent as the combustion process continued, especially at 50% and 90% MFB, where the methanol-blended fuel combusted significantly faster by 4.0 degrees and around 7.0 degrees, respectively.

The high latent heat of vaporization and laminar flame speed of methanol in the blended fuel result in shorter ignition delays. The higher latent heat of vaporization helps increase the charge density by cooling the charge more effectively (Sharma et al. 2019). Additionally, the acceleration of the burn rate is facilitated by the higher laminar flame speed of the methanol-blended fuel, particularly evident during the 50% – 90% MFB phase. The higher oxygen content in alcohol-blended fuels enhances the laminar flame speed of combustion and ensures more consistent burning compared to baseline fuel.

CONCLUSION

The results indicated that methanol-blended fuel significantly outperformed the baseline fuel in terms of flame burning progress. Across all heat transfer correlations, the methanol-blended fuel exhibited a superior rate of heat release (RoHR). This improvement was attributed to the characteristics of the methanol-blended fuel, which facilitated the combustion process, as evidenced during 50% and 90% of the mass fraction burned (MFB). The differences were notable, with the methanol-blended

fuel burning 4.0 and 7.0 degrees faster at 50% and 90% combustion, respectively. The complete combustion of methanol-blended fuel occurred significantly faster, at 15° aTDC, compared to 21.5° aTDC for the baseline fuel. Additionally, the peak pressure generated by methanol-blended fuel demonstrated lower cyclic variation compared to the peak pressure produced by the baseline fuel. The coefficient of variation (COV) values for methanol-blended fuel were measured at 5.49%, compared to 7.48% for the baseline fuel. This consistency can be attributed to the properties of methanol, including a significantly higher research octane number (RON) and oxygen content, which altered the flame pattern development and propagation, leading to more efficient combustion.

REFERENCES

Alexander, J., and Porpatham, E. 2019. Investigations on combustion characteristics of lean burn si engine fuelled with ethanol and lpg. *In IOP Conference Series: Earth and Environmental Science*, 265: 012020

Annand, W. J. D. 1963. Heat transfer in the cylinders of reciprocating internal combustion engines. *Proceedings of the Institution of Mechanical Engineers*, 177(1): 973–96.

Hairuddin, A.A, Wandel, A.P and Yusaf, T. 2013. Effect of different heat transfer models on a diesel homogeneous charge compression ignition engine. *International Journal of Automotive and Mechanical Engineering*, 8(1): 1292–1304.

Black, F. 1991. An overview of the technical implications of methanol and ethanol as highway motor vehicle fuels. *SAE Transactions*, 100:1161–90.

Brunt, M.F.J, Rai,H. and Emtage, A.L. 1998. The calculation of heat release energy from engine cylinder pressure data the calculation of heat release energy from engine cyl pressure data. *SAE Transactions*, 107:1596–1609.

Chansauria, P., and Mandloi, R. K. 2018. Effects of ethanol blends on performance of spark ignition engine - A review. *In Materials Today: Proceedings*, 5: 4066–77.

Chen, Z., Wang, L, Yuan, X., Duan,Q., Yang,B. and Zeng, K. 2019. Experimental investigation on performance and combustion characteristics of spark-ignition dual-fuel engine fueled with methanol/natural gas. *Applied Thermal Engineering*, 150(3):164–74.

Cooney, C., Worm, J. and Naber, J.D. 2008. The calculation of mass fraction burn of ethanol-gasoline blended fuels using single and two-zone models. SAE Technical Paper 2008-01-0320.

Dabbaghi, M. F., Baharom, M. B., Abdul Karim, Z. A. , A. Aziz, A. R, Mohammed, S.E. and, Zainal A., E.Z 2021. Comparative evaluation of different heat transfer correlations on a single curved-cylinder spark ignition crank-rocker engine. *Alexandria Engineering Journal*, 60 (3): 2963–78.

Eyidogan, M., Ozsezen, A.N, Canakci,M. and Turkcan, A. 2010. Impact of alcohol-gasoline fuel blends on the performance and combustion characteristics of an si engine. *Fuel*, 89 (10): 2713–20.

Heywood, J. B. 1988. Internal combustion engine fundamentals. McGraw-Hill.

Hohenberg, G. F. 1979. Advanced approaches for heat transfer calculations. SAE Technical Paper 790825.

Huang, J., Xiao, H., Yang, X., Guo, F. and Hu, X. 2020. Effects of methanol blending on combustion characteristics and various emissions of a diesel engine fueled with soybean biodiesel. *Fuel*, 282(12): 118734.

Iliev, S. 2015. A comparison of ethanol and methanol blending with gasoline using a 1-D engine model. *In Procedia Engineering*, 100:1013–22.

Köten, H., Karagöz, Y. and Balcı, Ö. 2020. Effect of different levels of ethanol addition on performance, emission, and combustion characteristics of a gasoline engine. *Advances in Mechanical Engineering*, 12(7).

Li, Y., Gong, J., Deng Y., Yuan, W., Fu, J. and Zhang, Bin. 2017. Experimental comparative study on combustion, performance and emissions characteristics of methanol, ethanol and butanol in a spark ignition engine. *Applied Thermal Engineering*, 115:53–63.

Mahmudul, H. M., Hagos, F.Y., Mukhtar, M.N.A., Mamat, R. and Abdullah, A.A. 2018. Effect of alcohol on diesel engine combustion operating with biodiesel-diesel blend at idling conditions. *In IOP Conference Series: Materials Science and Engineering*, 318.

Kumar, M.P, Pal, A. and Gautam, S. 2022. Investigation of combustion and emission characteristics of an si engine operated with compressed biomethane gas, and alcohols. *Environmental Science and Pollution Research*, 31(7): 10262-10272.

Paluri, B., and Patel, D. 2022. Combustion and performance characteristics of si engine with bioethanol blended fuels. *International Journal of Energy Research*, 46(15): 24454–64.

Qi, D. H., and Lee, C. F.. 2016. Combustion and emissions behaviour for ethanol–gasoline-

blended fuels in a multipoint electronic fuel injection engine. *International Journal of Sustainable* Energy, 35 (4): 323–38.

Sarkar, A., Chowdhuri, A.K, Bhowal, A.J and Mandal, B.K. 2012. The performance and emission characteristics of si engine running on different ethanol-gasoline blends. *International Journal of Scientific & Engineering Research*, 3(6).

Nikhil, S., Patel, C., Tiwari, N. and Agarwal, A.K. 2019. Experimental investigations of noise and vibration characteristics of gasoline-methanol blend fuelled gasoline direct injection engine and their relationship with combustion characteristics. *Applied Thermal Engineering*, 158(7).

Sharudin, H., Abdullah, N.R, Mamat, A.M.I., Badrulhisam, N.H. and Mamat, Ri. 2018. Application of alcohol fuel properties in spark ignition engine: A Review. *Jurnal Kejuruteraan,* si1 (7): 37–47.

Shawal, S., Goschutz, M., Schild, M., Kaiser, S., Neurohr, M., Pfeil, J., and Koch, T. 2016. High-speed imaging of early flame growth in spark-ignited engines using different imaging systems via endoscopic and full optical access. *SAE International Journal of Engines*, 9(2): 704-718.

Shawal, S., Meon, M. S., Saedon, J. B., Remeli, M. F., Nor, N. M., and Kaiser, S. A. 2020. Analysis of high-speed broadband flame chemiluminescence imaging in a SI engine. *IOP Conference Series: Materials Science and Engineering*, 788(1): 012060).

Shawal, S., Saedon, J., Meon, M. S., Mohamad Nor, N. H., Kaiser, S. A. 2020. imaging and post-processing of early combustion in a spark-ignition engine via endoscopic access. *Journal of Mechanical Engineering*, 9(1): 217-227.

Rosdi, S.M, Mamat, R., Yassin, M.H.M., Yusaf, T. F. and Khoirunnisa, F. 2022. Experimental investigation on combustion behaviour, performance and emission of fusel oil-gasoline blends using turbocharged si engine. *Journal of Mechanical Engineering and Sciences*, 16(1): 8788–8800.

Soyhan, H. S., Yasar, H., Walmsley, H., Head, B., Kalghatgi, G. T. and Sorusbay, C. 2009. Evaluation of heat transfer correlations for hcci engine modeling. *Applied Thermal Engineering*, 29 (2–3): 541–49.

Woschni, G. 1967. A universally applicable equation for the instantaneous heat transfer coefficient in the internal combustion engine. SAE Technical paper 670931.

Yıldız, M., and Çeper, B.A. 2017. Zero-dimensional single zone engine modeling of an si engine fuelled with methane and methane-hydrogen blend using single and double wiebe function: A comparative study. *International Journal of Hydrogen Energy*, 42(40): 25756–65.

*Syahar Shawal
School of Mechanical Engineering,
College of Engineering,
Universiti Teknologi MARA, Shah Alam,
Malaysia.

*Corresponding author; email: Syahar Shawal; syahar6595@uitm.edu.my

Received date : 25th May 2017
Accepted date : 14th September 2017
In Press date : 16th October 2017
Published date : XX